Available online at www.sciencedirect.com
SCIENCE DIRECT®
Journal of Hydrology 278 (2003) 64–75
Journal of Hydrology
www.elsevier.com/locate/jhydrol

Predicting preferential water flow in soils by traveling-dispersive waves

Liliana Di Pietro[a,*], Stéphane Ruy[a], Yvan Capowiez[b]

[a]*Unité 'Climat, Sol et Environnement', INRA Avignon, Domaine St Paul, Site Agroparc, 84914 Avignon Cedex 9, France*
[b]*UMR 'Ecologie des invertébrés', INRA Avignon, Domaine St Paul, site Agroparc, 84914 Avignon Cedex 9, France*

Received 22 February 2002; accepted 21 March 2003

Abstract

Rapid preferential drainage or by-pass flow of water and pollutants occurs in soil macropores such as burrows and channels formed by earthworm activity in soils. We show that preferential flow through these non-capillary pores can be described by a traveling-dispersive wave. This wave is the solution of a non-linear convective–dispersive equation (KDW model) that depends on three transport parameters: two are related to a convective celerity and the other one is a dispersive coefficient. We show that the flux–mobile water content relation is hysteretic and that it can be described by a non-linear function of the mobile water content and its first time derivative.

By combining the latter relation with the continuity equation we derive the KDW model. This model can be viewed as a second-order correction of the purely convective kinematic wave model. The dispersive term incorporates the large-scale effects of dissipative forces without resolving the small-scale conservation equations in detail. We further present numerical solutions for the signaling problem and a direct method for estimating model parameters. The model is validated with data obtained from laboratory infiltration experiments on soil columns. The experiments were carried out in repacked soil columns inoculated with *Allolobophora chlorotica* earthworms. Varying rainfall intensities were applied at the top surface of the columns with a rainfall simulator. Both the mean of mobile water content within the columns and the drainage hydrograph at the bottom were recorded in time. The parameters of the model were estimated from the experimental flux–mobile water content relation. A very good agreement was found between model prediction and experimental data.

Keywords: Preferential flow; Kinematic–dispersive wave model; Earthworm channels; Soil drainage hydrographs

1. Introduction

Usually, soils show a nearly continuous distribution of void sizes, ranging from micrometers to centimeters. The balance between forces driving the flow (pressure and gravity) and the resistance forces opposing it (friction between the solid walls and the fluid, and irreversible dissipation due to viscosity) determines the total inertial variation of the linear momentum carried by infiltrating water and thus the mean water velocity in soil pores. The prevalence of each one of these forces on water flow depends on the pore size and therefore the hydraulic

* Corresponding author.
E-mail address: lili@avignon.inra.fr (L. Di Pietro).

0022-1694/03/$ - see front matter © 2003 Elsevier Science B.V. All rights reserved.
doi:10.1016/S0022-1694(03)00124-0

behavior varies across void sizes. Channeling flow (by-pass or macropore flow) is a rapid transient physical phenomena occurring in the larger and predominantly vertical continuous soil pores.

Germann (1990) and Chen and Wagenet (1992) derived functional relations between the mean water flux and the mobile water content within the draining porosity, based, respectively, on Newton's law of shear and on channel flow approaches. Both approaches lead to non-linear single-valued functions between the flux and the mobile water content.

The combination of these relations with the continuity equation leads to a kinematic wave model for describing water flow in draining pores (Germann, 1985). Although the kinematic wave model usually overestimates preferential flow, it has shown to well approximate mobile water in structured soils (Germann et al., 1997; Mdaghri-Alaoui, 1998). Actually, dispersive effects implying attenuation of kinematic water waves are usually observed (Di Pietro and Lafolie, 1991; Di Pietro and Germann, 2001).

One factor contributing to wave attenuation is the role of mesopore flow. These pores of intermediate size may significantly contribute to channeling flow with typical time-scales ranging from a few hours to one or two days. Because in mesopores capillary forces may be significant, the contribution of mesopores to channeling flow is not exclusively gravity driven. In the operational classification of soil porosity proposed by Luxmoore (1981) into three main pore classes (micro-, meso- and macroporosity) mesopores ($10-1000\ \mu m$) and macropores ($>1000\ \mu m$) are both draining pores that differ in the time-scale for drainage and channeling flow. However, a non-arbitrary distinction between meso- and macropores is impossible to establish because the dominance of capillary forces diminishes gradually with the inverse of the equivalent pore radius while gravity remains constant. In what follows, we shall use the term 'draining porosity' to refer to the pores that may potentially contribute to relevant channeling flow. This functional criterion does not imply a quantitative division in terms of void size but it implies that some capillary dispersion must be considered in mainly gravity driven flow.

Channeling flow is typically unsteady. In transient flow regimes, the frictional and gravitational forces do not balance instantaneously (Majda, 1984). For rapidly varying transient flow regimes, as may occur in the larger pores, non-negligible inertial time lag forces develop to conserve total momentum. The local inertia of the mass of fluid in motion tends to slow the fluid down and is responsible for the attenuation of water waves.

In addition to capillary and time inertial effects, other forces, including spatial convective inertial effects and resistance forces due to intricate pore paths, may appear and produce water flow dispersion within the draining porosity (Di Pietro, 1998).

The aggregation of all damping effects culminates in a large-scale process being characterized as flow dispersion. The kinematic wave model is strictly convective and thus it is not able to account for dispersive effects whatever their origins, the reason being that it is based on the assumption that the flux is exclusively a function of the mobile water content. The underlying physical assumptions are the predominance of gravity driven flow over capillary forces, and that gravity is instantaneously counterbalanced by dissipative friction due to viscosity. No other dissipative forces are considered to act on the system. When non-conservative forces that induce dispersion are present, the flux also depends on the derivatives of the mobile water content (Lighthill and Whitman, 1955; Whitham, 1974; Singh, 1996).

In this paper a kinematic–dispersive wave (KDW) model is proposed to more accurately describe channeling flow through the draining soil porosity. In this case we assume that, among all the small-scale effects inducing dispersion, the local inertia force is prevalent in the greater pores and cannot be neglected. A way to incorporate the large-scale effect of this force without resolving the small-scale conservation equations in detail is to assume that the flux is some non-linear function of the mobile water content and of its first time derivative. The combination of this relation with the continuity equation leads to a convective–dispersive equation that admits traveling-dispersive wave solutions describing water infiltration into draining pores. We further present numerical solutions for the signaling problem and a direct method for estimating model parameters. The model is validated with data obtained from laboratory infiltration experiments on soil columns.

2. Theory

2.1. Kinematic–dispersive wave model for channeling flow through draining pores

Let w be the mobile volumetric water content within a volume V of a soil profile (flowing in the draining porosity), $w_t \equiv \partial w/\partial t$ its first partial derivative with time, and u the volumetric flux of mobile water normal to the external surface of V. We assume that the microporosity is entirely saturated and thus no water exchange exists between the two porosities.

The law of continuity for the flow of w may be expressed as

$$\frac{\partial w}{\partial t} + \nabla\cdot\mathbf{u} = 0 \tag{1}$$

If we further assume that the volumetric water flux u is some non-linear function of w and of w_t, that is

$$u = u(w, w_t) \tag{2}$$

then the spatial gradient of the flux results

$$\nabla\cdot u = c\nabla w + \nu_w \nabla w_t \tag{3}$$

where

$$c = \left.\frac{\partial u}{\partial w}\right|_{w_t=\text{constant}} \text{ and } \nu_w = \left.\frac{\partial u}{\partial w_t}\right|_{w=\text{constant}}$$

By assuming that water flow is only relevant in the vertical downward direction z, Eqs. (1) and (3), respectively, become

$$\frac{\partial w}{\partial t} + \frac{\partial u}{\partial z} = 0 \tag{4}$$

and

$$\frac{\partial u}{\partial z} = c\frac{\partial w}{\partial z} + \nu_w \frac{\partial^2 w}{\partial z \partial t} \tag{5}$$

Eqs. (4) and (5) can be combined to yield

$$\frac{\partial w}{\partial t} + c\frac{\partial w}{\partial z} = -\nu_w \frac{\partial^2 w}{\partial z \partial t} \tag{6}$$

Using $\partial^2 w/\partial z\partial t = -\partial^2 u/\partial z^2$ and multiplying by $\partial u/\partial w$, Eq. (6) is transformed into

$$\frac{\partial u}{\partial t} + c\frac{\partial u}{\partial z} = \nu_u \frac{\partial^2 u}{\partial z^2} \tag{7}$$

where $\nu_u = c\nu_w$.

Both Eqs. (6) and (7) are non-linear convective–dispersive equations, respectively, for w and u. Note that the functional form of the flux–mobile water content relation affects the hydrodynamic coefficients c, ν_u, and ν_w, but it does not alter the form of the obtained differential equations.

In this paper we shall concentrate on the solutions and the physical implications of Eq. (7) (KDW model in flux-mode) for channeling flow. The KDW model may be viewed as a second-order correction of the purely convective kinematic wave model that we discuss in Section 2.2. As we show later, the KDW model allows for a better macroscopic description for channeling flow.

2.2. The kinematic approximation

The two terms of the left-hand side in Eq. (7) represent the total time derivative of the flux $u(z,t)$ along any curve in the plane (z,t) with slope c at any point of it. These curves are called the characteristics of the differential equation. These terms may be written as

$$\frac{\mathrm{d}u}{\mathrm{d}t} = \frac{\partial u}{\partial t} + \frac{\mathrm{d}z}{\mathrm{d}t}\frac{\partial u}{\partial z} \tag{8}$$

with $c = \mathrm{d}z/\mathrm{d}t$. When $\nu_u = 0$, Eq. (7) reduces to

$$\frac{\mathrm{d}u}{\mathrm{d}t} = \frac{\partial u}{\partial t} + c(w)\frac{\partial u}{\partial z} = 0 \tag{9}$$

The latter is the kinematic wave model that has been widely applied in water resources modeling (see, for instance, the review by Singh (2001)).

Eq. (9) implies that $u(z,t)$ remains constant along the characteristic curves.

For the initial value problem

$$u = f(z), \qquad t = 0, \quad -\infty < z < \infty \tag{10}$$

the model admits continuous non-dispersive traveling wave solutions which propagate with speed $c(w)$ along the characteristics. If $f(z)$ is a decreasing function of z, discontinuities due to the overtaking of slower waves by faster ones may develop, allowing for the propagation of shock waves (Lax, 1972; Whitham, 1974).

Germann (1985) solved Eq. (9) for the signaling problem that corresponds to the following initial and

boundary conditions

$$\begin{cases} u(z,t) = u_{\text{in}}(t), & z = 0, \quad t > 0 \\ u(z,t) = u_0, & z > 0, \quad t = 0 \end{cases} \tag{11}$$

where $u_{\text{in}}(t)$ was a square input water pulse of volumetric flux density u_s and duration t_s applied at a free boundary ($z = 0$). He further assumed that the flux–mobile water content relation was $u = bw^a$, a and b [L T^{-1}] being two positive coefficients. The obtained analytical solutions indicate that the characteristics are straight lines corresponding to two shock waves that evolve without spreading. One originates from the applied flux at the surface u_s at time $t = 0$ (the wetting front) and the other one from the reduction to zero flux at the surface when input ceases at time $t = t_s$ (draining front). Furthermore, the draining front travels faster than the wetting front. After the draining front intercepts the wetting front, the solution $u(z,t)$ results in a single-crested function of time and the water content of the peak begins to decrease. Predicted hydrographs at the bottom of a soil

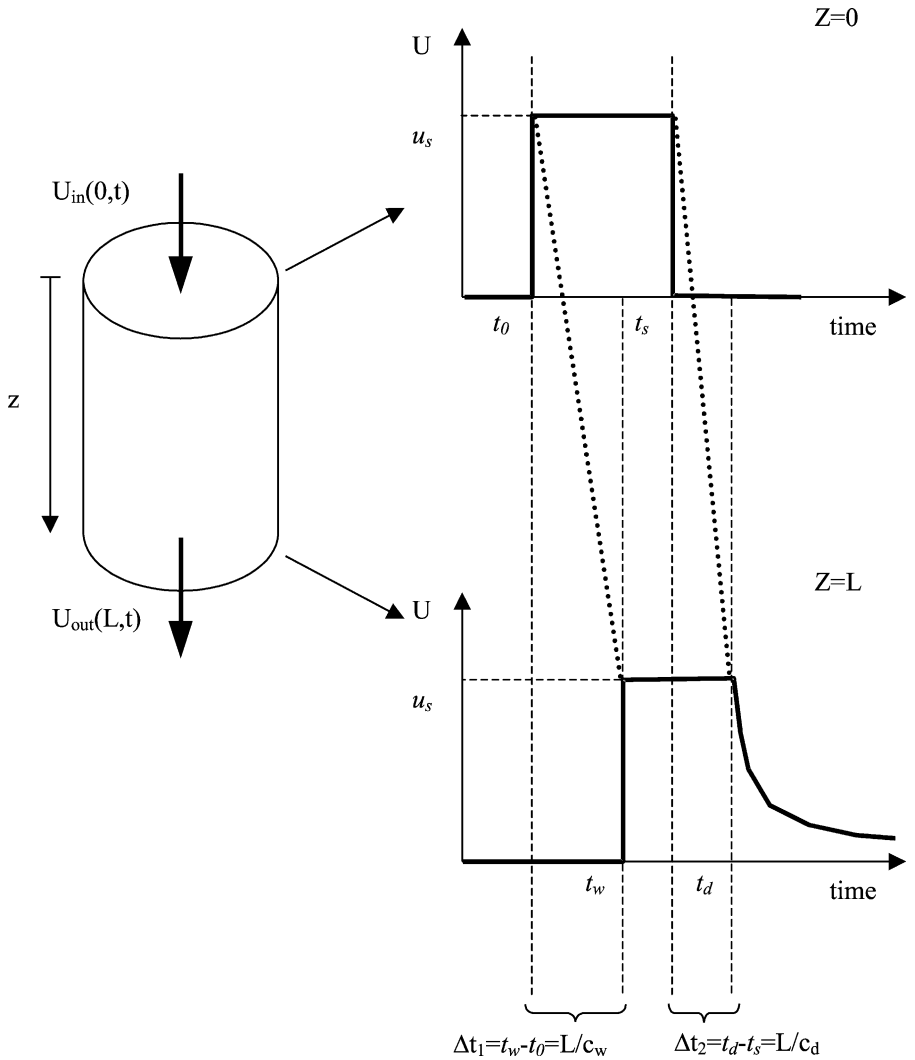

Fig. 1. Hydrographs at the bottom of a soil column (L) as predicted by the kinematic wave model (Germann, 1985) for an square water pulse input. Δt_1 and Δt_2 are the time lags expected for the arrival of the wetting and draining fronts that travel, respectively, with c_w and c_d as signal velocities.

column are shown schematically in Fig. 1. The time lag expected for the arrival of the wetting and draining fronts at depth L are, respectively, given by $\Delta t_1 = L/c_w$ and $\Delta t_2 = L/c_d$. The velocities c_w and c_d are the signal speeds that correspond to u_s and to $u = 0$, respectively.

In contrast to these predictions, experimental data obtained from soil columns and field lysimeters show that during the infiltration stage the hydrograph shows dispersion. As the signal advances in the (z,t) space, this effect is amplified and the kinematic approximation generally worsens (Di Pietro and Germann, 2001).

2.3. Implications of the second-order correction and numerical solutions for the signaling problem

When $\nu_u \neq 0$, the second-order term of the right-hand side of the Eq. (7) introduces dispersion. This differential equation is usually called the heat equation or the generalized Burges equation (Burges, 1948). By using Eq. (8), we may rewrite Eq. (7) to give

$$\frac{du}{dt} = \nu_u \frac{\partial^2 u}{\partial z^2} \tag{12}$$

Eq. (12) indicates that the flux u is no longer constant on each characteristic and that the rate of change depends on ν_u and on the spatial variation of the gradient of the flux.

It has been proved (Vanaja and Sachdev, 1992; Guilding and Kersner, 1996) that the occurrence of a free boundary (front or interface) in solutions of this type of non-linear convection-dispersion equation is equivalent to the admission of traveling-dispersive wave solutions.

We want to solve Eq. (7) and look for these traveling wave solutions for the case of an arbitrary infiltrating water signal applied to the surface of a porous medium presenting a network of draining pores (the microporosity is entirely saturated or it is impervious).

We shall further assume that the functional relation given in Eq. (2) is of the form

$$u = f(w) + g(w_t) \tag{13}$$

with $f(w) = bw^a$, and $g(w_t) = -\nu_w(\partial w/\partial t)$, where a, b [L T^{-1}], and ν_w [L] are positive real numbers. Eq. (13) is proposed to model the experimental results we obtained from infiltration–drainage experiments in many soil columns. The observed $u(w)$ curves are hysteretic, the values of u for a fixed value of w being smaller during infiltration than during drainage. Our hypothesis is that an inertial force develops during the transient stages of infiltration and drainage, to counterbalance the increase (respectively, the decrease) of linear momentum. This force is proportional to the rate of increase (respectively, the decrease) of the water content, and is zero during steady state. The corrective term $g(w_t)$ is proportional to the first temporal derivative of the water content. This term $g(w_t)$ is negative during infiltration (w increases), zero during steady state (w remains constant) and positive during drainage (w decreases). As discussed by Lighthill and Whitman (1955), when a flux-density relation like $u(w)$ shows hysteresis, the area between the rising and falling curves provides an estimate to correct for dispersion.

From Eq. (13), the signal speed c results

$$c(w) = \left.\frac{\partial u}{\partial w}\right|_{w_t=\text{cte}} = mw^n \tag{14}$$

with $n = a - 1$ and $m = ab$.

Further

$$\nu_u = c\nu_w = mw^n\nu_w \tag{15}$$

Under the above assumptions, c reduces to the first-order kinematic approximation of Germann (1985, 1990) who ignored $g(w_t)$.

Using $w = (u/b)^{1/a}$ and by combining Eqs. (7), (13) and (14), we obtain

$$\frac{\partial u}{\partial t} + pu^q \frac{\partial u}{\partial z} = \nu_w p u^q \frac{\partial^2 u}{\partial z^2} \tag{16}$$

where

$$p = ab^{1/a} \text{ and } q = \frac{a-1}{a} \tag{17}$$

Thus the model depends on the three parameters p, q, and ν_w. The first and the second are combinations of the parameters a and b in Eq. (13) and are related with the first-order kinematic signal speed.

We have solved Eq. (16) numerically for the initial and boundary conditions given by Eq. (11) by applying an explicit finite difference scheme.

The numerical derivation is described in Appendix A. The program was written in *Mathematica* language.

3. Comparison of numerical results with real infiltration experiments in soil columns with macropores

3.1. Experimental layout

Infiltration–drainage experiments were carried out on uniformly packed soil columns inoculated with earthworms. A PVC column (height = 283 mm, diameter = 153.6 mm) was filled with 2–4 mm aggregates of a loamy soil. To insure a homogeneous distribution, the aggregates were carefully packed in successive layers following the procedure of Capowiez et al. (2001). Each layer (600 g of soil) was compacted with a hydraulic press by applying a pressure of 270 kPa. The thickness of each layer was about 2.5 cm. To increase cohesion between layers the surface of each layer was gently scraped using a small rake prior to adding a new layer. The total initial bulk density and the total porosity of the soil column were, respectively, 1.11 g cm^{-3} and 0.57 m^3 m^{-3}.

Four *Aporrectodea chlorotica* earthworms were introduced into the soil, which was stored under controlled humidity and temperature conditions for three months. Columns were lined inside with sealing varnish and sharp fine sand to prevent earthworms crawling along the walls instead of burrowing in the soil. The cores were placed in a dark room (at 12 °C) for

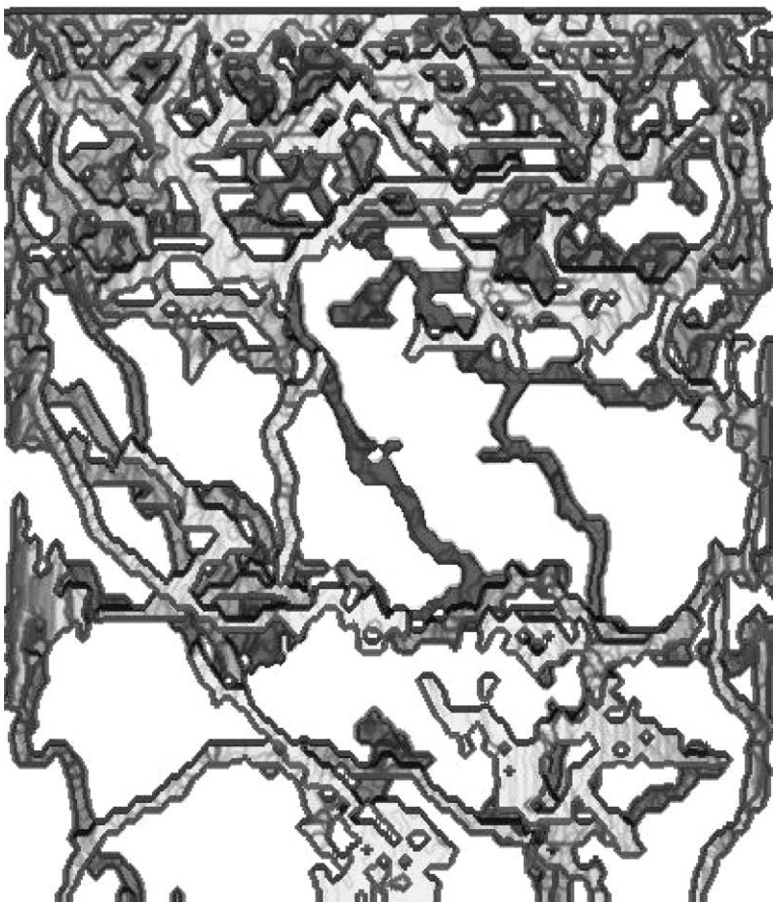

Fig. 2. 3D reconstruction of the burrow system for the soil column inoculated with 4 *Ap. chlorotica* earthworms. Light and dark grey, respectively, represent the background and foreground planes.

6 weeks. During this period the earthworms built connected macropore networks within the soil column.

A semi-qualitative characterization of the form and the connectivity of the macropore network was obtained by X-ray tomography. The cores were scanned with an X-ray scanner (Prospeed SX Advantage, General Electric) to obtain a set of images 2 mm thick every 3 mm with a resolution of 0.4 mm per pixel. The settings for the X-ray beam were 140 mA, 130 kV and a duration of 1 s. A three-dimensional reconstruction of the macroporosity within the column (Fig. 2) was obtained by the method presented in Pierret et al. (2002).

Prior to the infiltration experiments, the column was saturated from below for 72 h with distilled water and allowed to drain freely to constant weight. Then little water exchange between microporosity and draining porosity is expected.

A funnel was then sealed on to the bottom of the column and the whole device was placed on a weighing scale (Sartorius FC34EDE, Sartorius AG, Goettingen, Germany, maximum range = 34 kg, precision = ±0.1 g) as shown in Fig. 3. This device allowed for continuous monitoring of the mass variation of the soil columns during the infiltration–drainage experiment.

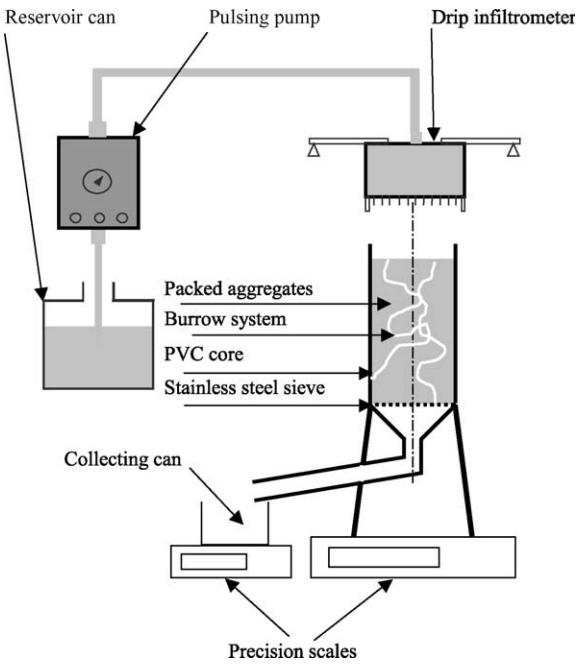

Fig. 3. Experimental scheme of the infiltration–drainage experiments.

Water was provided at the top surface of the column with a drip infiltrometer fed by a pulsing pump connected to a reservoir tank of distilled water (Bruckler et al., 2002). Infiltration intensity provided by the drip infiltrometer can be adjusted between 4 mm h^{-1} to more than 500 mm h^{-1}.

Drainage flow was continuously monitored with a weighing scale (Mettler-Toledo PM2000, Viroflay, France, maximum range = 2 kg, precision = 0.01 g).

We carried out three infiltration runs with simulated constant rainfall intensities of 30.35, 56.07 and 101.66 mm h^{-1} and durations 0.55, 0.30, and 0.33 h, respectively.

3.2. Estimation of the parameters of the model

Parameters p, q and v_w were estimated from the experimental $u(w)$ relation, with u measured at the base of the column, and w estimated as an average for the whole column.

The parameters p and q are related to parameters a and b through Eq. (17). In the first-order kinematic approximation $u(w)$ is a single-valued function of w and is equal to $f(w) = bw^a$. We plotted u as a function of w during the infiltration and drainage cycles for the three experiments (Fig. 4). The $u(w)$ relation is

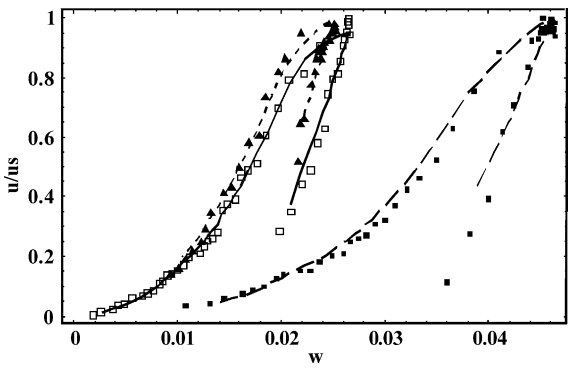

Fig. 4. Relative flux (u/u_s) vs. mobile water content for the three input intensities (u_s). Symbols are for measured fluxes and lines for fitted values (Eq. (13)): triangles and dashed line: 30.35 mm h^{-1}, squares and full line: 56.07 mm h^{-1}, filled squares and long dashed line: 101.66 mm h^{-1}.

Table 1
Estimated parameters for the three infiltration experiments

Rainfall intensity (mm h^{-1})	a (–)	b (mm h^{-1})	ν_w (mm)	RMS (mm h^{-1})	p	q
30.35	2.15	83 079	71	0.88	417	0.535
56.07	2.15	131 682	73	1.52	517	0.535
101.66[a]	2.88	707 407	70	4.37	309	0.653

Parameters a, b and ν_w were estimated from the best fit of the experimental $u(w)$ curves to the model (Eq. (13)). The values of p and q are calculated from Eq. (17). RMS is the root mean square error.
[a] Convergence not reached.

hysteretic, the values of u for a fixed value of w being smaller during infiltration than during drainage. This shows that the first-order approximation that considers $u(w) = f(w)$ is not well adapted to describe the complexity of the process. We assume that Eq. (13) describes the observed experimental relation and the hysteretic loop. In order to estimate the parameters involved in Eq. (13), we minimize the root mean square of the deviations between the experimental data and the flux predicted by Eq. (13), as follows

$$\mathrm{RMS} = \sqrt{\frac{1}{N}\sum_i \left(u_i - \left(bw_i^a - \nu_w \left.\frac{\partial w}{\partial t}\right|_i\right)\right)^2}$$

where N, u_i, w_i are, respectively, the number of experimental observations, the observed fluxes at the bottom of the column at time i and the mean of the measured mobile water content at time i. The derivatives $\partial w/\partial t$ were approximated by forward finite differences from the experimental data. The estimated parameters for each run are presented in Table 1. For these experiments, the higher is the rainfall intensity the higher is the value of parameter b whereas ν_w remains nearly constant. Furthermore, the values of parameter a are between 2 and 3 as predicted by kinematic theory (Germann, 1985). Nevertheless more experiments should be carried out to confirm these trends. As seen in Fig. 4, relation (13) fits the experimental data reasonably well.

3.3. Comparisons of model predictions with experimental data

For all the infiltration runs, and irrespectively of the rainfall intensity, the drainage hydrographs always exhibit the same shape: a rapid increase changing into a plateau when a steady state is reached followed by a steep decrease when the input flux has ceased. The falling stage is characterized by an abrupt initial drop in outflow rate followed by a period of slow drainage (Fig. 5). During the infiltration stage, the rising hydrograph shows dispersion. We observe that dispersion of the wetting front decreases when the input rate increases. At higher intensities, some small-scale dispersive effects like local water stagnation or capillary effects within pores of intermediate size are probably masked, and the coarser pores mostly contribute to channeling flow involving higher velocities. In the latter case, the hypothesis of non-dispersive shock-wave propagation is probably more accurate.

The statistical model efficiency (EF) was used to evaluate the performance of the model:

$$\mathrm{EF} = 1 - \frac{\sum_{i=1}^{N}(P_i - O_i)^2}{\sum_{i=1}^{N}(\overline{O} - O_i)^2}$$

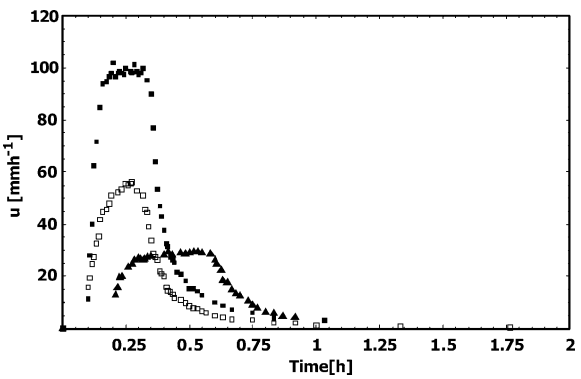

Fig. 5. Comparison of the experimental drainage hydrographs at the bottom of the soil column for three water input rates: 30.35 mm h^{-1} (triangles), 56.07 mm h^{-1} (squares) and 101.66 mm h^{-1} (filled squares).

Table 2
Efficiency criterion for cross-simulation of experiment j (column) using the optimal parameters obtained from experiment k (row)

Parameters	Experiment		
	30.35 (mm h^{-1})	56.07 (mm h^{-1})	101.66 (mm h^{-1})
30.35 (mm h^{-1})	0.951	0.848	0.824
56.07 (mm h^{-1})	0.960	0.942	0.823
101.66 (mm h^{-1})	0.954	0.903	0.827

where P_i and O_i represent predicted and observed fluxes, and $\overline{O}$ is the mean of the observed fluxes. The ideal value of EF is 1. The lower is the value of EF with respect to 1 the poorer is the fit. Table 2 shows the EF values obtained for cross-simulations of experiment j using the parameters estimated from experiment k, respectively, with $k \equiv j = 1, 2, 3$.

The best fit between predicted and observed data is obtained with the parameters obtained from the intermediate input rate $u(w)$ curve (56.07 mm h^{-1}). Nevertheless, the EF values obtained with the two other set of parameters are very close to the optimal values and model predictions do not significantly differ as shown in Fig. 6. Numerical solutions are in reasonable agreement with experimental data although dispersion of the rising limb of the hydrograph for the highest input rate is somewhat overestimated. Model predictions worsen with the increase of the input rate. This confirms the hypothesis that dispersive effects progressively fade out as input rates increase.

Fig. 7(a)–(c) shows the numerical solution of the KDW model estimated with the optimal parameters, the experimental data, and the analytical solution of the first-order kinematic model of Germann (1985). The arrival times of the wetting and drainage fronts at the bottom of the column are well predicted by both models and coincide. Dispersive effects do not change the convective speed of the traveling wave but they affect its shape, attenuating the rising stage and sharpening the falling stage of the hydrograph.

To compare the accuracy of the KDW model with respect to the kinematic model, we calculated the squared deviations of the predicted and measured values for both models. The cumulative squared deviations as a function of time are shown in

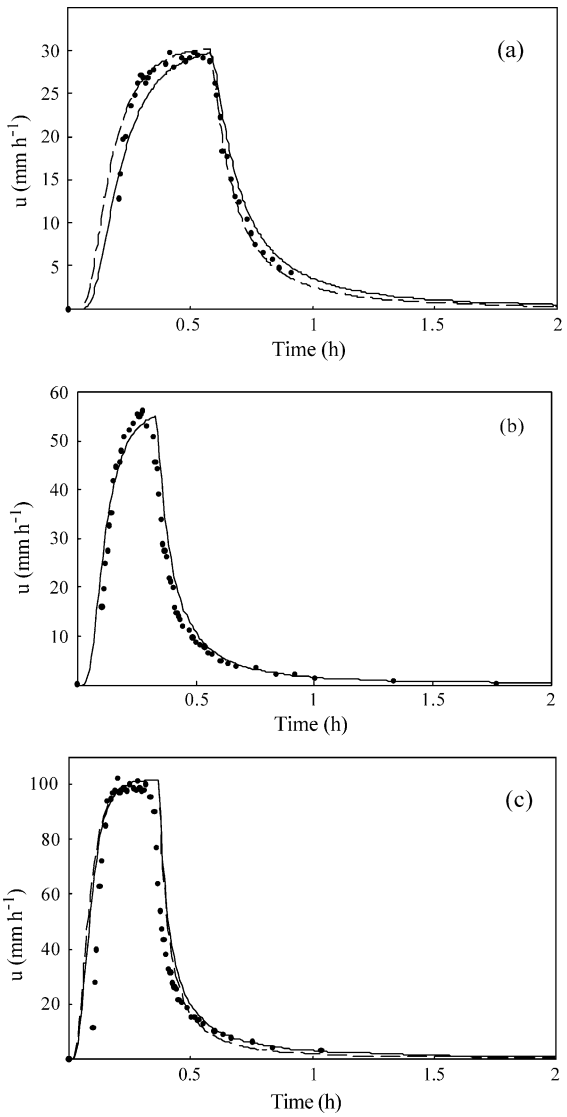

Fig. 6. Measured (dots) and predicted hydrograph by the KDW model (lines) at the bottom of the column for the three input intensities. (a) 30.35 mm h^{-1}; (b) 56.07 mm h^{-1}; (c) 101.66 mm h^{-1}. Dashed line: simulation with the parameters estimated from the 56.07 mm h^{-1} experiment ('optimal parameters'). Full line: simulation with the parameters estimated from the experiment.

Fig. 7(d)–(f). We observe that both models predict better the falling than the rising stage of the hydrograph. Still the KDW model substantially improves the accuracy of the prediction in both stages with respect to the kinematic wave model.

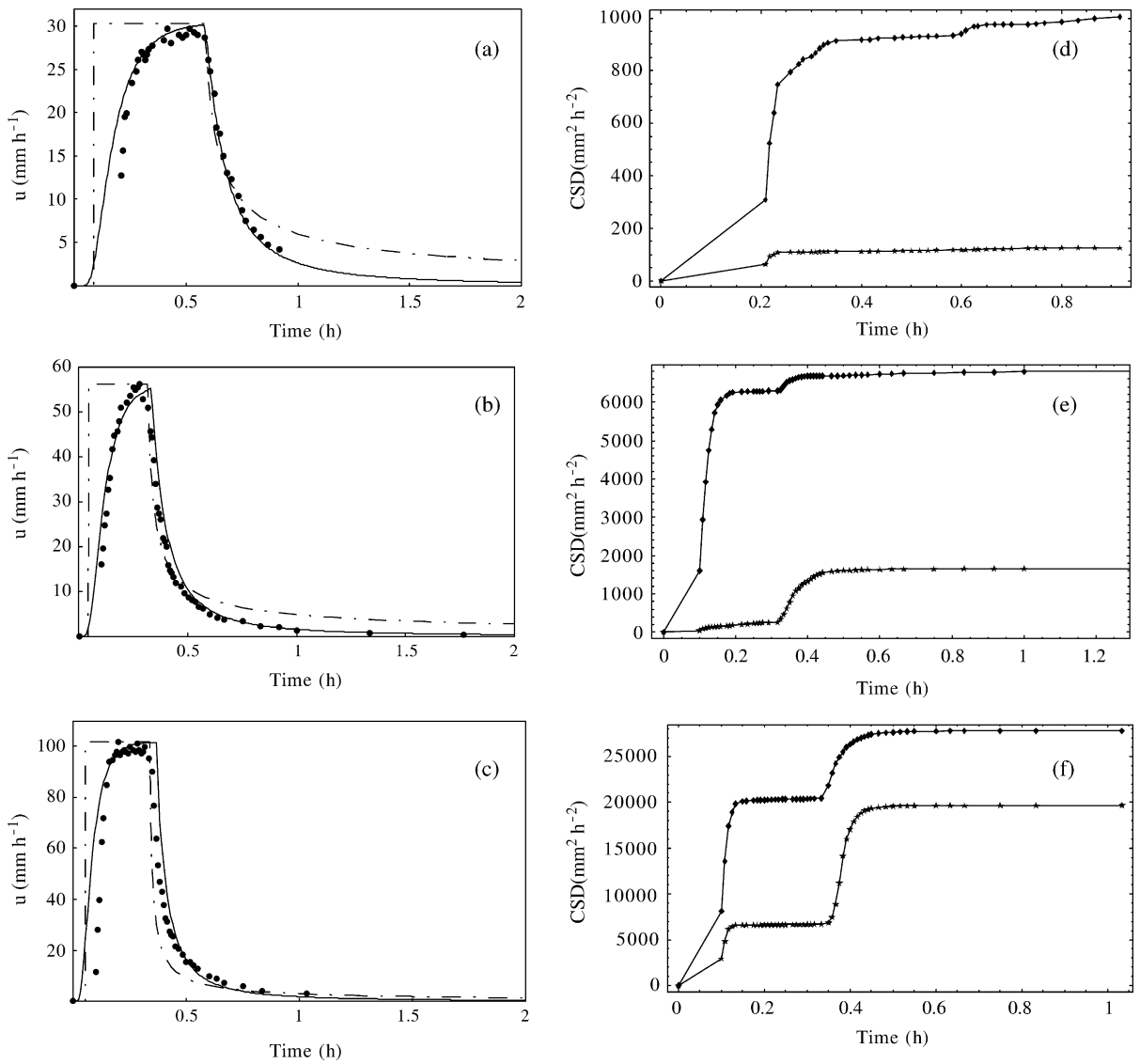

Fig. 7. Experimental drainage hydrographs at the bottom of the soil column (dots), hydrographs simulated with KDW model (full lines), and analytical solution given by the first-order kinematic wave model (dashed lines) of Germann (1985). Figures on the right represent the cumulative square deviations between measured and predicted fluxes with model KDW (stars) and with the first-order kinematic model (diamonds). (a) and (d) 30.35 mm h^{-1}; (b) and (e) 56.07 mm h^{-1}; (c) and (f) 101.66 mm h^{-1}.

3.4. Sensitivity analysis

We carried out numerical simulations to analyze the influence of parameters a, b, and ν_w on the outflow hydrographs predicted by the KDW model. Fig. 8 shows the calculated root mean square of the deviations between the optimal solution and those obtained by varying each parameter. The RMS$-\nu_w$, RMS$-a$, and RMS$-b$ curves are, respectively, asymmetrical. They increase more rapidly for negative than for the positive variations of the parameters. Within the range of variation analyzed,

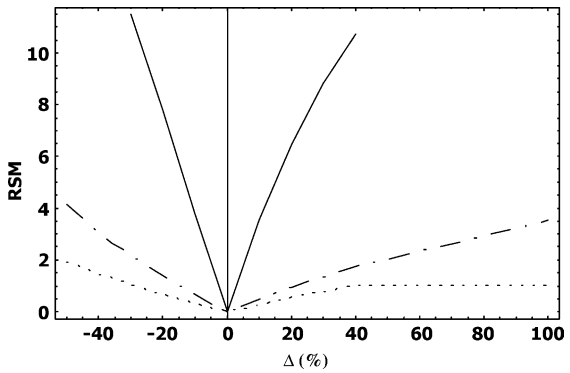

Fig. 8. Sensitivity analysis performed on parameters a (full line), b (dashed line) and ν_u (dotted line) for the 56.07 mm h^{-1} experiment. RMS: root mean square of the deviations with respect to the optimal values.

the RMS$-\nu_w$ curve seems to reach a plateau for values of ν_w higher than 108 mm (50% of positive variation with respect to the optimal value).

Small positive or negative variations of coefficient a lead to significant variations on the outflow hydrographs. The influence of variations of b and of ν_w is less marked but still significant.

4. Conclusions

In this study we developed a new infiltration model that describes channeling flow within soil macropores. The KDW model is based on the kinematic-wave theory and it incorporates dispersive effects. We performed infiltration–drainage experiments on large soil columns inoculated with *Ap. chlorotica* earthworms. At the time of the experiments structural characteristics of the burrow systems were computed from X-ray CAT scanning. The earthworms formed a connected network of macropores that was reconstructed with a 3D algorithm. These experiments were used to estimate the relation between the volume water flux and the mobile water content. This relation has been shown to be hysteretic and it could be modeled by a non-linear function of the water content and its first derivative. Experimental data were also used to test the model. We have shown that the KDW model accurately predicts the drainage hydrographs for various input rates. In this paper we did not consider water exchange between the macro- and microporosity. In the future we shall study the influence of different initial water content values on model parameters.

Appendix A. Numerical approximation

Eq. (16) is discretised using a fully explicit scheme in time and space (Ganzha and Vorozhtsov, 1996). The time derivative is approximated by a forward difference and space derivatives are approximated by central differences at the jth time step. Eq. (16) becomes

$$u_i^{j+1} = u_i^j + \frac{\tau\nu_w}{h^2}c(u)(u_{i+1}^j - 2u_i^j + u_{i-1}^j) - \frac{\tau}{2h}c(u)(u_{i+1}^j - u_{i-1}^j) \quad \text{(A1)}$$

where subscript i is for space discretisation, superscript j is for time discretisation, h is the space interval, τ is the time step, and $c(u)$ is the convective celerity which is a function of u.

h and τ are automatically calculated by the program in order to satisfy the following stability condition:

$$\left(\left(\frac{\tau}{h}\right)c(u)\right)^2 \le 2\frac{\tau\nu_w}{h^2}c(u) \le 1 \quad \text{(A2)}$$

The stability condition is evaluated for $u = u_s$.

By using Eq. (14) the relation between c and u is expressed as:

$$c = \frac{ab}{b^{(a-1)/a}}u^{(a-1)/a} \quad \text{(A3)}$$

As u is time and space dependant, the celerity must be evaluated at each time step and each space interval. As the input signal is very discontinuous and as the celerity vanishes for $u = 0$, the choice of the time step and the space interval at which c is evaluated is critical for the good propagation of the input signal through space. After several trials, we chose to evaluate c at $u_{i-0.5}^{j+0.5}$:

$$c = \frac{ab}{b^{(a-1)/a}}\left(\frac{u_i^j + u_{i-1}^{j+1}}{2}\right)^{(a-1)/a} \quad \text{(A4)}$$

References

Bruckler, L., Bertuzzi, P., Angulo-Jaramillo, R., Ruy, S., 2002. Testing an infiltration method for estimating soil hydraulic properties in the laboratory. Soil Science Society of America Journal, 66(2), 384–395.

Burges, J., 1948. A mathematical model illustrating the theory of turbulence. Advances in Applied Mechanics 1, 171–199.

Capowiez, Y., Monestiez, P., Belzunces, L., 2001. Earthworm burrow systems made by *A. nocturna* and *A. chlorotica* in artificial cores: morphological differences and effects of interspecific interactions. Soil Applied Ecology 16, 109–120.

Chen, C., Wagenet, R.J., 1992. Simulation of water and chemicals in macropore soils: representation of the macropore influence and its effect on soil water flow. Journal of Hydrology 130, 105–126.

Di Pietro, L., 1998. Strategies for describing preferential flow: the continuum approach and cellular-automaton fluids. In: Selim, H.M., Ma, L. (Eds.), Physical Nonequilibrium in Soils, Modeling and Application. Ann Arbor Press, Chelsea, Michigan, pp. 437–453.

Di Pietro, L., Germann, P., 2001. Testing kinematic wave solutions for flow in macroporous soils against a lattice-gas simulation. Soil Science Society of America Journal 56, 147–168. Special Publication No. 56.

Di Pietro, L., Lafolie, F., 1991. Water flow characterization and test of a kinematic wave model for macropore flow in a highly contrasted and irregular double-porosity medium. Journal of Soil Science 42, 551–563.

Ganzha, V.G., Vorozhtsov, E.V., 1996. Numerical Solutions for Partial Differential Equations: Problem Solving Using Mathematica. CRC Press, New York, pp. 347.

Germann, P., 1985. Kinematic wave approximation to infiltration and drainage into and from soil macropores. Transactions ASAE 28, 745–749.

Germann, P., 1990. Preferential flow and the generation of runoff: boundary layer flow theory. Water Resources Research 26 (12), 3055–3063.

Germann, P., Di Pietro, L., Singh, V., 1997. Momentum of flow in soils assessed with TDR-moisture readings. Geoderma 80, 153–168.

Guilding, B.H., Kersner, R., 1996. The characterisation of reaction–convection–diffusion processes by travelling waves. Journal of differential equations 124 (1), 27–79.

Lax, P., 1972. The formation and decay of shock waves. American Mathematical Monthly 79, 227–241.

Lighthill, M., Whitman, G., 1955. On kinematic waves. I. Flood movement in long rivers. Proceedings of the Royal Society, London, Series A, 281–316.

Luxmoore, R.J., 1981. Comments on micro, meso, and macroporosity of soil. Soil Science Society of America Journal 45 (3), 671–672.

Majda, A., 1984. Compressible fluid flow and systems of conservation laws in several space variables, Applied Mathematical Sciences, 53. Springer, New York.

Mdaghri-Alaoui, A., 1998. Transferts d'eau et de substances dans des milieux non saturés à porosité bimodale: expérimentation et modélisation, Thesis, Universität Bern, Bern, pp. 143.

Pierret, A., Capowiez, Y., Belzunces, L., Moran, C.J., 2002. 3D reconstruction and quantification of macropores using X-ray computed tomography and image analysis. Geoderma, 106, 247–271.

Singh, V.P., 1996. Kinematic wave modeling in water resources: surface-water hydrology. Wiley, New York.

Singh, V., 2001. Kinematic wave modelling in water resources: a historical perspective. Hydrological processes 15, 671–706.

Vanaja, V., Sachdev, L., 1992. Asymptotic solutions of a generalized Burgers equation. Quarterly of Applied Mathematics 1 (4), 627–640.

Whitham, G.B., 1974. Linear and non-linear waves. Wiley, New York.